Catalysis Today 172 (2011) 203–208

Contents lists available at ScienceDirect

Catalysis Today

journal homepage: www.elsevier.com/locate/cattod

Ni and W interactions in the oxide and sulfide states on an Al_2O_3–TiO_2 support and their effects on dibenzothiophene hydrodesulfurization

Alida Elizabeth Cruz-Perez[a], Alfredo Guevara-Lara[a,*], Judith Pilar Morales-Ceron[a], Alejandro Alvarez-Hernandez[a], José Antonio de los Reyes[b], Laurence Massin[c], Christophe Geantet[c], Michel Vrinat[c]

[a] Área Académica de Química, Universidad Autónoma del Estado de Hidalgo, Carr. Pachuca-Tulancingo Km. 4.5, Ciudad Universitaria, C.P. 42184, Pachuca, Hidalgo, Mexico
[b] División de Ciencias Básicas e Ingeniería, Universidad Autónoma Metropolitana-Iztapalapa. Av. San Rafael Atlixco No. 186, Col. Vicentina, Iztapalapa, C.P. 09340, D.F., Mexico
[c] Institut de Recherches sur la Catalyse et de l'Environnent de Lyon, IRCELYON, UMR 5256 CNRS/Université Lyon 1, 2 Av. Albert Einstein- F-69626- Villeurbanne Cedex, France

ARTICLE INFO

Article history:
Received 7 December 2010
Received in revised form 1 March 2011
Accepted 1 March 2011
Available online 13 April 2011

Keywords:
DBT HDS
Ni–W catalysts
Ni^{2+}–$W_{12}O_{41}{}^{10-}$ heteropolyoxometalate
TiO_2–Al_2O_3

ABSTRACT

In order to determine the species distribution at different steps of catalyst preparation, NiW/TiO_2–Al_2O_3 catalysts were prepared by aqueous impregnation with solutions at pH = 4 and 9, respectively. Raman and UV–Vis diffuse reflectance spectroscopies for Ni–W/TiO_2–Al_2O_3 precursors showed that during impregnation step $Ni^{2+}{}_{Oh}$–$W_{12}O_{41}{}^{10-}$ entities were formed for pH = 4 and 9. After calcination, $Ni^{2+}{}_{Oh}/WO_4{}^{2-}$ and $Ni^{2+}{}_{Oh}$–$W_{12}O_{41}{}^{10-}$ species were identified for solids synthesized at pH = 4 and at pH = 9, respectively. Calcined catalyst impregnated at pH 4 displayed the highest Dibenzothiophene (DBT) hydrodesulfurization (HDS) activity for this series. This high activity was related to a higher concentration for the NiWS phase for the catalyst prepared at pH = 4 than that at pH = 9, as evidenced by X-ray photoelectron spectroscopy (XPS). It could be suggested that impregnation at pH = 9 allowed a high Ni–W interaction, forming $Ni^{2+}{}_{Oh}$–$W_{12}O_{41}{}^{10-}$ precursor and consequently, an inefficient sulfidation. Besides, for catalyst impregnated at pH 4, $Ni^{2+}{}_{Oh}/WO_4{}^{2-}$ precursor underwent a more complete transformation to NiWS phase and led to a higher DBT HDS activity.

1. Introduction

Environmental specifications require diesel and gasoline fuels with less than 50 ppm of sulfur content. Then, hydrodesulfurization processes need catalysts able to remove the refractory molecules such as dibenzothiophene and 4,6 dimethyl-dibenzothiophene [1]. Industrial hydrodesulfurization uses conventional NiMo/Al_2O_3 and CoMo/Al_2O_3 catalysts, while NiW catalysts are less common. However, it has been reported [2–4] that the NiW catalysts show several advantages in the alkyl-dibenzothiophene transformation.

The relationship between structure and catalytic activity for HDS catalysts containing Co (Ni)-promoted MoS_2(WS_2) clusters supported on γ-Al_2O_3 could be associated to the "CoMoS" or "NiWS" phases, as suggested by Topsøe et al. [5]. The CoMoS phase was shown to be MoS_2-like structures with the promoter (Co or Ni) atoms located at the edges planes of MoS_2 in five-fold coordinated sites [5]. Furthermore, these authors claim that a single slab structure (called Type-I Co–Mo–S) interacts strongly with the support, probably via Mo–O–Al linkages located at the edges for the alumina-supported catalysts, whereas for the multiple slab form (called Type-II CoMoS) these interactions are smaller [5].

To our knowledge, there are only a few studies about Ni–W/TiO_2–Al_2O_3 interactions [6–9]; nonetheless, Ni–Mo studies could be used as references. Shimada et al. [10] reported that the structure orientation is also very important to achieve the maximal dispersion for catalytically CoMoS active phase. Furthermore, these authors claim that MoS_2 clusters supported on TiO_2 (anatase) are edge-bonded multiple MoS_2 clusters. These structures contribute to overcome the steric hindrance for the sulfur compounds on the catalyst surface. In addition, Van Veen et al. [11] reported that TiO_2 did not adsorb Mo species, but provoked formation of Mo superficial precipitate. Regarding Al_2O_3 support, Sakashita [12] reported that edge-bonded oriented structures could be formed early during the impregnation and calcinations steps. From their results, it appeared that the edge-bonded molybdenum oxides clusters (MoO_n) supported on a γ-Al_2O_3 single crystal thin maintained their orientation after sulfidation at low temperature. However, if the sulfidation was carried out at high temperature the structures with edge-bonded MoS_2 clusters were transformed into basal-bonded multiple- and mono- slab MoS_2 clusters. Therefore, supports are

* Corresponding author. Tel.: +52 771 717 2000x2202; fax: +52 771 717 2000x6502.
E-mail address: guevaraa@uaeh.edu.mx (A. Guevara-Lara).

0920-5861/$ – see front matter © 2011 Elsevier B.V. All rights reserved.
doi:10.1016/j.cattod.2011.03.027

required to confer stability to the edge-bonded MoS_2 clusters, which induce maximum dispersion for catalytic active sites.

For NiMo/γ-Al_2O_3 and NiW/γ-Al_2O_3 catalysts differences in sulfidation behavior have been reported [6] and these differences are closely related to the Ni and Mo (or W) impregnated precursors, on which depends the formation of "NiWS" phase. Breysse et al. [13,14] reported that sulfiding at 673 K for WO_x/Al_2O_3 was limited and, that there was a small amount of W that presented higher oxidation state either as oxysulfides or as WS_3 species. In addition, it was reported [12,15,16] that sulfidation for WO_3 and MoO_3 to WS_2 and MoS_2, proceeded through oxysulfides as intermediates [17–21]. Ramirez [22] reported that W–Al_2O_3 interaction increased with the calcination temperature and thus leading to a more difficult sulfidation.

The combination of a high interaction between W or Mo and Al_2O_3 species and the low interaction Mo–TiO_2 suggest that the active phase-support interaction for a catalyst supported on Al_2O_3–TiO_2 mixed oxide carrier could be modify, in order to produce a highly active NiW catalyst.

In a previous paper [23], dealing with Ni–Mo/TiO_2–Al_2O_3 catalysts, a 95%TiO_2–5%Al_2O_3 support was impregnated with a solution containing MoO_4^{2-} and $[Ni^{2+}4O^{2-}]$ species. The point of zero charge for the support (PZC = 6) provoked a polymerization from Ni–Mo species in solution leading to close Ni–Mo interactions according to Eq. (1).

$$7MoO_4^{2-} + 8H^+ + Ni^{2+} \underset{\text{solutionat pH=9}}{\overset{TiO_2-Al_2O_3}{\rightleftarrows}} Ni^{2+}/Mo_7O^{6-} + 4H_2O \quad (1)$$

Uncalcined samples led to the highest HDS activity through this synthesis procedure, considering that the impregnation pH was relevant to the preparation for the active phase. Based on these observations, in this work we focused on the pH impregnation effect for NiW supported species on the active phase-support interactions and their influence on the DBT HDS activity.

2. Experimental

2.1. Preparation of TiO_2–Al_2O_3 support

A TiO_2–Al_2O_3 mixed oxide support with 5 mol% of Al_2O_3 was prepared by precipitation method. Aluminum isopropoxide (solid) was dissolved directly into the titanium isopropoxide (liquid), and then stirred during 4 h at T = 25 °C. The precipitate was obtained by hydrolysis of the previous mixture with drop-wise addition of deionized water. Then, the obtained precipitate was dried at 120 °C for 12 h, and then calcined at 550 °C (5 °C min^{-1}) for 6 h.

2.2. Synthesis of NiW/TiO_2–Al_2O_3 catalysts

In order to obtain catalysts with 19 wt% WO_3 and 4 wt% NiO, the support (100–150 mesh) was co-impregnated, using the incipient wetness method, with an aqueous solution of $(NH_4)_6H_2W_{12}O_{40}xH_2O + Ni(NO_3)_26H_2O$. Impregnation was performed at natural pH of 4, or the pH solution was adjusted to 9 by addition of an aqueous 0.01 M NH_4OH solution. These solids were kept at room temperature for 24 h and then dried at 120 °C for 12 h and calcined at 400 °C (5 °C/min) for 4 h. The solids were characterized and evaluated, before and after the calcination step, respectively. Catalysts were named as indicated in Table 1.

2.3. Catalysts characterization

TiO_2–Al_2O_3 support was characterized by N_2 physisorption and ζ-potential. N_2 physisorption was carried out on an ASAP 2020 Micromeritics apparatus. Previously to measurement, the samples were treated at 300 °C during 4 h under vacuum at $P = 30 \times 10^{-6}$ mmHg. Specific surface area was obtained by application of the Brunauer, Emmet and Teller (BET) equation and porous size was calculated from desorption isotherm by BJH method. ζ-potential measurements were performed using a Malvern ZetaSizer 3000 apparatus; 0.05 g of support was dispersed in 1 L of a 0.1 M KOH electrolytic solution at 25 °C. pH was adjusted with a 0.01 M of aqueous NH_4OH or HNO_3 solution. Catalysts in oxidic state were characterized by Raman and UV–Vis diffuse reflectance (UV–Vis DRS) spectroscopies. Raman spectra were recorded on a Perkin Elmer GX Raman FT-IR apparatus equipped with a Nd:YAG (1064 nm) laser and an InGaAs detector. For each spectrum, an average of 10-50 scans were obtained with a laser power of 40–300 mW in the 1500–100 cm^{-1} range, 2–4 cm^{-1} resolution. UV–Vis diffuse reflectance spectra (UV–Vis DRS) were obtained on a Perkin Elmer Lambda 40 spectrometer equipped with an integration sphere. As UV–Vis DRS reference, we used the Spectralon SRS-99-010 (99% reflectance) tablet. Data are shown as the Kubelka–Munk ($F(R_\infty)$) function:

$$F(R_\infty) = \frac{(1 - R_\infty)^2}{2R_\infty} \quad (2)$$

in which R_∞ is the reflectance at infinite depth.

Sulfided catalysts were characterized by X-ray photoelectron spectroscopy (XPS). XPS measurements were performed using an ESCALAB 200 R instrument equipped with an energy source of AlKα, E = 1486.6 eV.

Table 1
Nomenclature of prepared catalysts.

Catalyst	pH impregnation	Treatment
NiW(4)-NC	4.0	Dried at 120 °C
NiW(9)-NC	9.0	Dried at 120 °C
NiW(4)-C	4.0	Calcined at 400 °C
NiW(9)-C	9.0	Calcined at 400 °C
NiWS(4)-NC	4.0	Dried and sulfided
NiWS(9)-NC	9.0	Dried and sulfided
NiWS(4)-C	4.0	Calcined and sulfided
NiWS(9)-C	9.0	Calcined and sulfided

2.4. Catalytic tests

Catalysts were activated by sulfidation with a 4 L/h flow of 10 mol% H_2S/H_2 gas mixture, at 360 °C (5 °C/min) during 4 h. Catalysts were tested in the hydrodesulfurization of gasoline model (500 PPM S correspond to a mixture of 0.37 mol dibenzothiophene/n-heptane). Tests were carried out in a continuous flow trickle-bed micro-reactor with 0.05 g of catalyst at T = 300 °C and P = 30 bar. The reactor was fed with a 1.2×10^{-4} L/h of gasoline and 2.2 L/h of H_2 (STP) flows. As an internal standard for gas chromatography, dodecane was added to the liquid feed in the same molar amount as DBT. Heptane was selected as solvent because under the reaction conditions: T = 300 °C and P = 30 bar, all reactants are in gas phase [24]. Liquid samples were analyzed by gas chromatography on a Perkin Elmer AutoSystem instrument equipped with a FID detector and a HP-Ultra 2 (30 m × 0.32 mm i.d.) column. Main reaction products were biphenyl and cyclohexylbenzene. Reaction rates were calculated considering first order kinetics and a differential reactor as follows:

$$r_i = \frac{F_{i_0} x_i}{m_c} \quad (3)$$

where, F_{i_0} = feed DBT molar flow, m_c = catalyst weight, x_{DBT} = DBT conversion.

$$x_{DBT} = \frac{C_{DBT_0} - C_{DBT}}{C_{DBT_0}} = \frac{\sum A_i}{\sum A_i + A_{DBT}} \quad (4)$$

where, A_i = peak area of i products in the chromatogram.

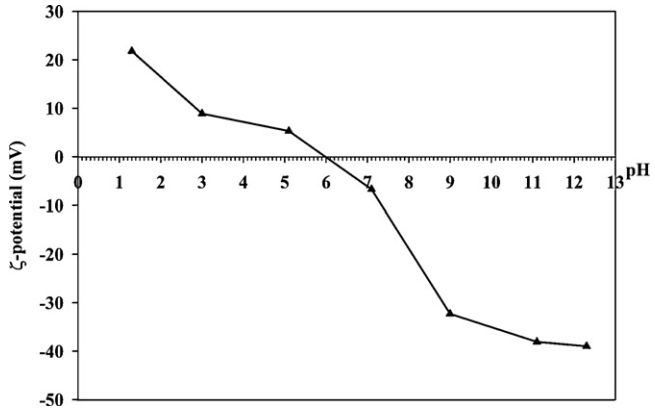

Fig. 1. ζ-Potential of TiO_2–Al_2O_3 colloidal solution as a function of pH. $T = 25\,^{\circ}C$.

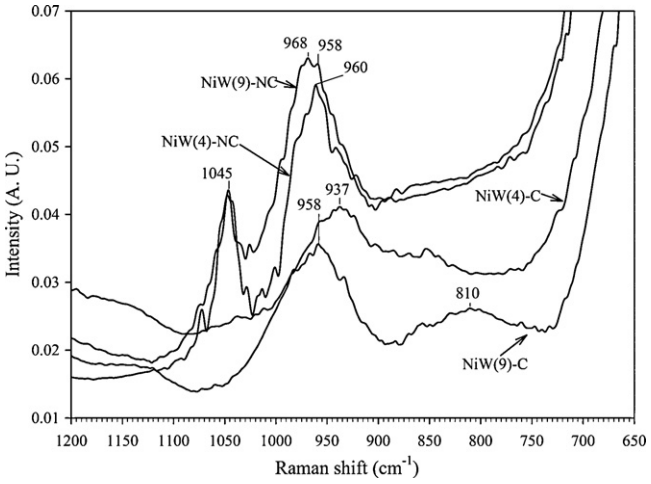

Fig. 2. Raman spectra of NiW/TiO_2–Al_2O_3 catalysts. –NC, Non calcined. –C, calcined.

3. Results and discussion

3.1. TiO_2–Al_2O_3 support characterization

A specific superficial area (A_{BET}) of 220 m^2/g, a porous volume of 0.4 cm^3/g and a mean porous diameter of 7 nm were obtained from N_2 physisorption data.

During the impregnation step, the behavior of surface charge depends on oxide–water interphase and consequently, it has an effect on the superficial Ni and W distribution. The establishment of surface charge may occur by two distinct but essentially equivalent mechanisms [25]: i) the adsorption of protons or hydroxyls at amphoteric sites, Eq. (5). And, ii) the formation in solution of hydroxylated metal species, which are deposited on the surface according to Eqs. (6–8).

$$MOH_2^+ \xleftarrow{H^+} MOH \xrightarrow{OH^-} MO^- + H_2O \quad (5)$$

$$M^{n+} + xOH^- \rightarrow M(OH)_x^{(n-x)^+} \ldots \quad (6)$$

$$M(OH)_x^{(n-x)^+} + OH^- \rightarrow M(OH)_{x+1}^{(n-x-1)^+} \ldots \quad (7)$$

$$M(OH)_x^{(n-x)^+} + H^+ \rightarrow M(OH)_{x-1}^{(n-x+1)} + H_2O \ldots \quad (8)$$

The point of zero charge (PZC) method relies on assumption that if the solid is placed in a solution with the same pH as PZC it will cause no change in that pH. Normally, the PZC is obtaining by titration. On the other side, the isoelectric point (IEP) is obtained when the ζ-potential is 0 and, the fact that it is independent of the ionic strength of the KOH suggests that: (i) KOH is an indifferent electrolyte in this system and (ii) the IEP is in this case the same as the PZC and consequently, the same that the net surface pH [25]. TiO_2 anatase phase presents an IEP of 5.8 and γ-Al_2O_3 an IEP of 8.0; however, the surface charge depends on the structure and preparation method of the supports. Fig. 1 shows that the TiO_2–Al_2O_3 has an IEP equal to 6, in agreement with previous results [24–26].

3.2. Nickel and tungsten oxide species supported on TiO_2–Al_2O_3 characterization by Raman and DRS

From the literature data [23,27–32], W species show 800–980 cm^{-1} Raman bands for the W=O terminal bond, while W–O–W vibration modes appear between 200 and 800 cm^{-1}. However, TiO_2 anatase structure presents Raman bands at 640, 510, 390 and 200 cm^{-1} [33]. For this reason, only the W=O terminal bond Raman band will be discussed.

The pH = 4 aqueous solution for impregnation contains $W_{12}O_{40}^{8-}$ [30], $Ni^{2+}{}_{Td}$ and $Ni^{2+}{}_{Oh}$ ions [23,34,35] while the pH = 9 aqueous solution contains WO_4^{2-} [30] and $Ni^{2+}{}_{Td}$ [23,34,35] entities. TiO_2–Al_2O_3 support having an IEP of 6, the species which were present in the solution at pH = 4 should be maintained after the impregnation. On the contrary, WO_4^{2-} species contained in pH = 9 solution should be polymerized to $W_{12}O_{40}^{8-}$. From these results, Raman spectra for NiW/TiO_2–Al_2O_3 catalysts impregnated at pH = 4 and 9 could be explained. Fig. 2 depicts these spectra for dried (–NC) and calcined (–C) samples. A band is observed at 1045 cm^{-1} and it is related to NO_3^- ions [36], which disappear after the calcination step.

Indeed, the NiW(9)-NC catalyst shows a 958–968 cm^{-1} wide band, corresponding to W=O symmetric stretching vibrations for $W_{12}O_{40}^{8-}$. The TiO_2–Al_2O_3 isoelectric point (IEP = 6) causes a polymerization from WO_4^{2-} monomers in pH = 9 solution onto supported $W_{12}O_{40}^{8-}$. The NiW(4)-NC catalyst shows a 960 cm^{-1} band that is related to $W_{12}O_{40}^{8-}$ ion. This polytungstate impregnated with a pH = 4 solution remains during the impregnation step. Both NiW(9)-NC and NiW(4)-NC catalysts exhibit $W_{12}O_{40}^{8-}$ polyoxometalate species, but Raman shift differences suggest that the impregnation at pH = 9 allows a polytungstate different from that in $(NH_4)_6(H_2W_{12}O_{40}) \times H_2O$ salt. For the NiW(4)-C catalyst a 937 cm^{-1} band is associated to WO_4^{2-} monomer and suggests that during the calcination step, the $W_{12}O_{40}^{8-}$ polyoxometalate is segregated into WO_4^{2-} monomers. For the NiW(9)-C catalyst 958 and 810 cm^{-1} bands, are associated to $W_{12}O_{40}^{8-}$ and WO_3 species, respectively.

In literature, UV–Vis diffuse reflectance (UV–Vis RD) spectra for tungsten-based catalysts in the oxidic state generally show 200–400 nm bands, which correspond to tungsten oxides species with tetrahedral symmetry (260–280 nm) and octahedral symmetry (300–320 nm) [37]. However, for alumina–titania supported catalysts, these bands may be overlapped with the bands caused by $O^{2-} \rightarrow Ti^{4+}$ charge transfer of TiO_2 in this region [33]. Then, only the region between 500 and 1100 nm can be used to determine the local symmetry for supported nickel ions.

Ni^{2+} ion with local tetrahedral symmetry ($Ni^{2+}{}_{Td}$) presents 376, 623 and 977 nm bands in (Ni + Mo) solution [23]. However, these bands could be shifted due to Ni-support or Ni–W interactions [34,38,39]. The presence of $Ni^{2+}{}_{Td}$ could be associated to the formation of $NiAl_2O_4$ [38,39] and $NiTiO_3$ [40] spinels.

Ni^{2+} ion with local octahedral symmetry ($Ni^{2+}{}_{Oh}$) presents 393, 659 and 731 nm bands in (Ni + Mo) solution [23] and 390–409, 630–671, 705–757 nm bands for Ni-support or Ni–W interactions [23,34,38,39]. $Ni^{2+}{}_{Oh}$ ion could be related to a Ni–W interaction [23,41–43].

UV–Vis diffuse reflectance spectra of our NiW catalysts are given in Fig. 3, in which the bands corresponding to Ni^{2+} ion in

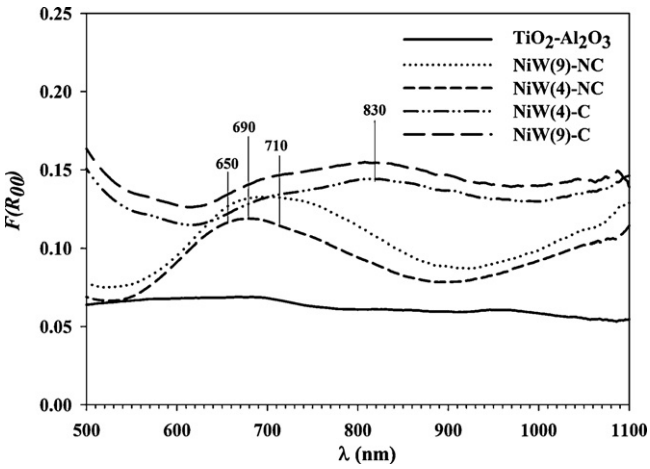

Fig. 3. UV–Vis diffuse reflectance spectra of NiW/TiO_2–Al_2O_3 catalysts.

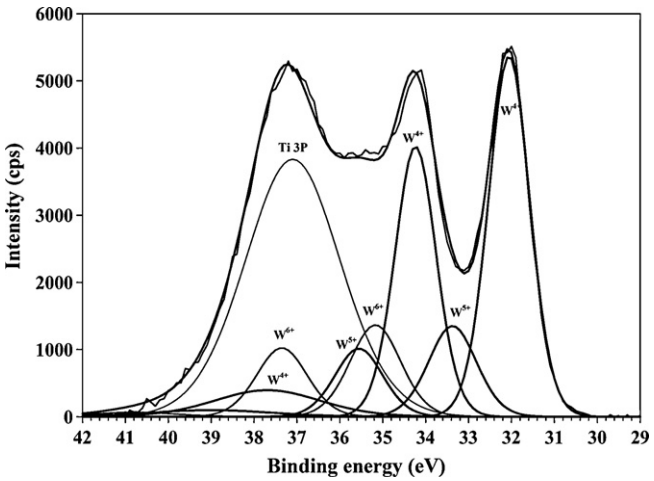

Fig. 4. W 4f spectra of NiWS(4) catalyst.

solution are also reported as reference. NiW(4)-NC presents a band at 680 nm which is associated to $Ni^{2+}{}_{Oh}$ distorted symmetry [23,38,43]. NiW(9)-NC also presents a wide band between 680 and 760 nm that corresponds to $Ni^{2+}{}_{Oh}$ distorted symmetry, suggesting a high distortion of Ni^{2+} ion symmetry during the pH = 9 impregnation. In addition to Raman results, $Ni^{2+}{}_{Td}$ and $WO_4{}^{2-}$ monomers were polymerized to $Ni^{2+}{}_{Oh}$–$W_{12}O_{40}{}^{8-}$ heteropolyoxometalate, in which the Ni^{2+} species are trapped in the $W_{12}O_{40}{}^{8-}$ structure. In the case of pH = 4 impregnation, $W_{12}O_{40}{}^{8-}$ polyoxometalate maintains its structure and the $Ni^{2+}{}_{Oh}$ ion is adsorbed onto the $W_{12}O_{40}{}^{8-}$ structure, possibly as $NiW_{12}O_{40}{}^{6-}$ heteropolyoxometalate. For calcined catalysts (NiW(4)-C and NiW(9)-C samples), Fig. 3 shows that UV–Vis RD spectra present a wide 680–830 nm band, suggesting that calcination step allows a high Ni^{2+} distortion of octahedral symmetry. This is probably due to a Ni–W close interaction. In addition of Raman results, NiW(9) catalyst presents $Ni^{2+}{}_{Oh}$–$W_{12}O_{40}{}^{8-}$ impregnated species. During pH = 9 impregnation, HO^- hydroxyls present in solution could saturate the support surface and do not allow the adsorption of Ni and W species. Then, polymerization induces a very close Ni–W interaction and, on contrary, a poor Ni-support interaction. Consequently, $Ni^{2+}{}_{Oh}$–$W_{12}O_{40}{}^{8-}$ and WO_3 are obtained during the calcination step. On the other side, NiW(4) catalyst presents $Ni^{2+}{}_{Oh}/WO_4{}^{2-}$ species obtained from $Ni^{2+}{}_{Oh}/W_{12}O_{40}{}^{8-}$. In this case, the Ni–W interaction allows an adequate W-support interaction that induces the segregation of $Ni^{2+}{}_{Oh}/W_{12}O_{40}{}^{8-}$.

3.3. Dibenzothiophene hydrodesulfurization tests

Ni–W precursor species are affected by impregnation pH and calcination process, and these different steps are expected to control the catalytic activity. Table 2 resumes the results obtained for dibenzothiophene hydrodesulfurization. NiWS(4)-NC and NiWS(9)-NC catalysts, which were sulfided without previous calcination, showed a similar reaction rate. The NiWS(9)-NC having an improvement to hydrogenation pathway. The calcination causes a favorable effect over the reaction rate, NiWS(4)-C and NiWS(9)-C catalysts showed a higher activity as compared with its homologues sulfided without previous calcination. In addition, the selectivity showed an increase in the direct desulfurization pathway. These results suggest that the $Ni^{2+}{}_{Oh}/WO_4{}^{2-}$ precursor phase onto NiWS(4)-C catalyst allows to obtain a higher activity than $Ni^{2+}{}_{Oh}$–$W_{12}O_{41}{}^{10-}$ heteropolyoxometalate onto NiWS(9)-C catalyst. However, it is difficult to associate the oxidic precursors with the activity of the sulfided phases.

3.4. X-ray photoelectron spectroscopy for NiW/TiO_2–Al_2O_3 catalysts

The catalytic activity differences between catalysts impregnated at pH 4 and 9 suggest some differences between the Ni and W sulfided species. X-ray photoelectron spectra for NiWS(4)-C and NiW(9)-C catalysts are reported in Figs. 4 and 5, respectively. The spectral region contains a Ti 3p peak and three W 4f doublets. W $4f_{7/2}$ and $4f_{5/2}$ doublet with binding energies at 32.1 and 34.3 eV is associated to W^{4+} for WS_2 phase [9,14,43]. The doublet with 33.3 and 35.3 eV binding energies is correlated to W^{5+} for oxysulfide WOS_x phase [44] and, the doublet with binding energies at 35.4 and 37.6 eV is associated to W^{6+} for WO_3 species [8,9,14]. Results obtained from decomposition of W 4f core level spectra, suggest that NiWS(4)-C sample is better sulfided than NiWS(9)-C catalyst (see Table 3). The WO_3 quantities suggest that sulfidation process was carried out more efficiently over $Ni^{2+}{}_{Oh}/WO_4{}^{2-}$ than over $Ni^{2+}{}_{Oh}$–$W_{12}O_{41}{}^{10-}$ heteropolyoxometalate. In addition, NiWS(4)-C catalyst shows a higher percentage of WOS_x phase than NiWS(9)-C catalyst.

Figs. 6 and 7 display the Ni 2p photoelectron spectra for NiWS(4)-C and NiW(9)-C catalysts. The spectral region contains three Ni $2p_{3/2}$ peaks and their respective satellites. The binding energy at 852.9 eV is related to NiS_x species [8]; at 853.7 eV is associated to NiWS phase [45] and at 855.9 eV is related to NiO_x [46] species, respectively. Table 3 shows that the NiWS(4)-

Table 2
Dibenzothiophene hydrodesulfurization on NiW/TiO_2–Al_2O_3 catalysts. T = 300 °C, P = 30 bar.

Catalyst	x_{DBT} (%)	Rate 10^{-8} (mol s^{-1} g^{-1})	Selectivity (%)	
			Biphenyl	Cyclohexylbenzene
NiWS(4)-NC	70.6	31	68	32
NiWS(9)-NC	60.7	29	59	41
NiWS(4)-C	96.6	46	81	19
NiWS(9)-C	80.9	39	75	25

Table 3
Atomic percentage obtained from decomposition of W4f and Ni2p core level spectra of NiWS/TiO_2–Al_2O_3 catalysts.

Catalyst	W 4f			Ni 2P			Ni/(Ni + Mo)	S/(Ni + W)	W/(Ti + Al)	Ni/(Ti + Al)
	WS_2% (W^{4+})	WOS_x % (W^{+5})	WO_3% (W^{6+})	NiS_x %	NiWS %	NiO_x %				
NiWS(4)-C	63	18	19	29	41	30	0.41	1.05	0.15	0.11
NiWS(9)-C	52	12	36	29	35	36	0.45	1.02	0.13	0.10

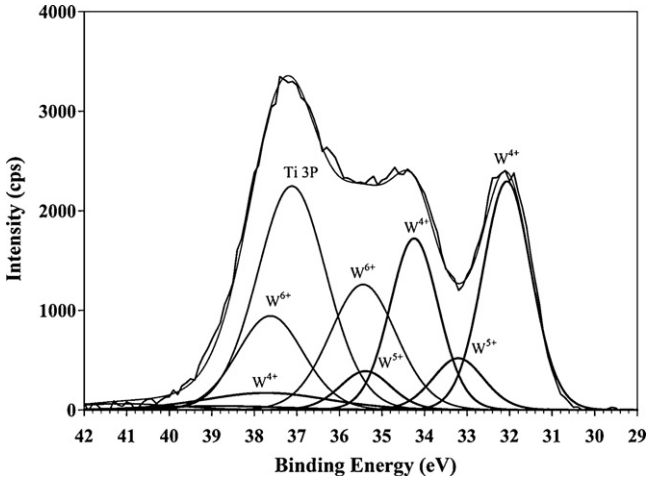

Fig. 5. W 4f spectra of NiWS(9) catalyst.

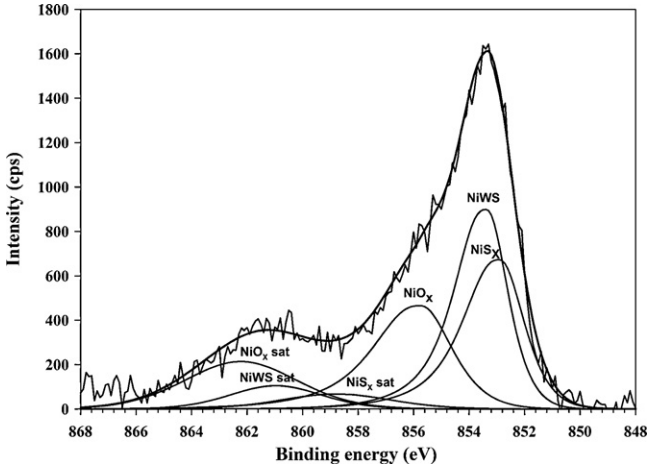

Fig. 6. Ni 2p spectra of NiWS(4) catalyst.

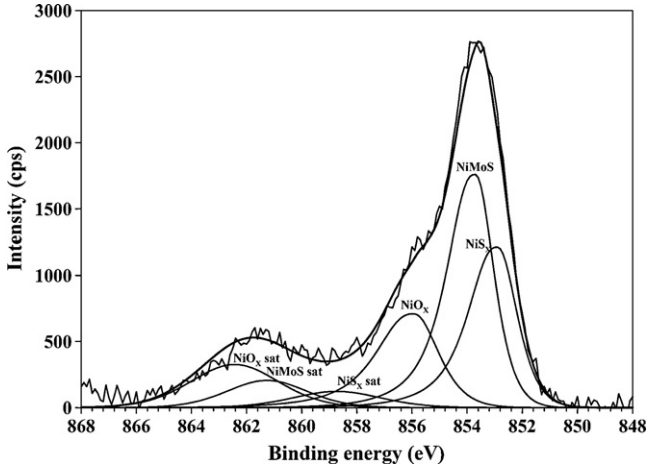

Fig. 7. Ni 2p spectra of NiWS(9) catalyst.

C contains a higher amount of NiWS phase than the NiW(9)-C catalyst. NiO_x concentration differences suggest the Ni^{2+} into $Ni^{2+}{}_{Oh}/WO_4{}^{2-}$ structure is easier sulfided than the Ni^{2+} contained into $Ni^{2+}{}_{Oh}$–$W_{12}O_{41}{}^{10-}$ structure.

XPS results allow the analysis of surface concentrations as atomic ratios (see Table 3). Ni/(Ti + Al), W/(Ti + Al), S/(Ti + Al) ratios indicate that the Ni and W dispersions are similar on NiWS(4)-C than on NiWS(9)-C catalyst. On the other side, the Ni/(Ni + W) ratio suggests that Ni dispersion is better on NiWS(4)-C catalyst. In addition, after sulfidation step, the higher amount of NiWS phase obtained for the NiWS(4)-C sample, indicate that the $Ni^{2+}{}_{Oh}/WO_4{}^{2-}$ entities favors the NiWS phase dispersion better than the $Ni^{2+}{}_{Oh}$–$W_{12}O_{41}{}^{10-}$ precursor.

4. Conclusions

The impregnation with a basic solution followed by the calcination process allows the formation of $Ni^{2+}{}_{Oh}$–$W_{12}O_{41}{}^{10-}$ heteropolyoxometalate with high Ni–W interaction. These entities are not efficiently sulfided under our work conditions, leading therefore to a lower catalytic activity. On the contrary, an impregnation at pH = 4 followed by the calcination process leads to $Ni^{2+}{}_{Oh}/WO_4{}^{2-}$ heteropolyoxometalate which can be more easily sulfided, leading to a higher amount of NiWS phase and then a higher catalytic activity was obtained.

In a previous work [23], we demonstrated that the NiMo system over a similar support presents a different behavior, since the NiMoS(9)-NC catalyst showed the highest concentration for the NiMoS phase and the highest activity. Therefore, sulfidation behavior is different between the Ni–W and Ni–Mo systems. Ni–Mo catalyst requires an impregnation at pH 9 to get a better interaction in order to prevent the segregation of phases during sulfidation. In the case of Ni–W systems, the impregnation at pH 9 causes a high Ni–W interaction which leads to an inefficient sulfidation and thus, to a lower concentration of the NiWS phase.

Acknowledgements

Authors acknowledge Mexico and the European Community for financial support for this research through FONCICYT contract No. 96164.

References

[1] H. Schulz, W. Böhringer, F. Ousmanov, P. Waller, Fuel Proc. Tech. 61 (1999) 5.
[2] W.R.A.M. Robinson, J.A.R. van Veen, V.H.J. de Beer, R.A. Santen, Fuel Proc. Tech. 61 (1999) 103.
[3] H.R. Reindhoudt, R. Troost, A.D. van Langeveld, S.T. Sie, J.A.R. van Veen, J.A. Moulijn, Fuel Proc. Tech. 61 (1999) 133.
[4] T. Kabe, Y. Aoyama, D. Wang, A. Ishihara, W. Qian, M. Hosoya, Q. Zhang, Appl. Catal. A 209 (2001) 237.
[5] H. Topsøe, B.S. Clasusen, F.E. Massot, Hydrotreating Catalysis: Science and Technology, Springer-Verlag, Berlin Heidelberg, 1996.
[6] E.J.M. Hensen, Y. van der Meer, J.A.R. van Veen, J.M. Niemantsverdriet, Appl. Catal. A 322 (2007) 16.
[7] M. Breysse, M. Cattenot, T. Decamp, R. Frety, C. Gachet, M. Lacroix, C. Leclercq, L. de Mourgues, J.L. Portefaix, M. Vrinat, M. Houari, J. Grimblot, S. Kasztelan, J.P. Bonnelle, S. Housni, J. Bachelier, J.C. Duchet, Catal. Today 4 (1988) 36–55.
[8] A. Spojakinaa, R. Palchevaa, K. Jiratovab, G. Tyulieva, L. Petrova, Catal. Lett. 104 (2005) 45.
[9] D. Zuo, M. Vrinat, H. Nie, F. Mauge, Y. Shi, M. Lacroix, D. Li, Catal. Today 93 (2004) 751.

[10] H. Shimada, Catal. Today 86 (2003) 17.
[11] J.A.R. Van Veen, P.A.J.M. Hendriks, Polyhedron 5 (1986) 75.
[12] Y. Sakashita, Surf. Sci. 489 (2001) 45.
[13] M. Breysse, J. Bachelier, J.P. Bonnelle, M. Cattenot, D. Cornet, T. Decamp, J.C. Duchet, P. Engelhard, R. Frety, C. Gachet, P. Geneste, J. Grimblot, C. Gueguen, S. Kasztelan, M. Lacroix, J.C. Lavalley, C. Leclercq, C. Moreau, L. De Mourgues, J.L. Olive, E. Payen, J.L. Portefaix, H. Toulhoat, M. Vrinat, Bull. Soc. Chim. Belg. 96 (1987) 829.
[14] M. Breysse, M. Cattenot, T. Decamp, R. Frety, C. Gachet, M. Lacroix, C. Leclercq, L. de Mourgues, J.L. Portefaix, M. Vrinat, M. Houari, J. Grimblot, S. Kasztelan, J.P. Bonelle, S. Housni, J. Bachelier, J.C. Duchet, Catal. Today 4 (1988) 39.
[15] A.J. van der Vlies, G. Kishan, J.W. Niemantsverdriet, R. Prins, T. Weber, J. Phys. Chem. B 106 (2002) 3449.
[16] A.J. van der Vlies, R. Prins, T. Weber, J. Phys. Chem. B 106 (2002) 9277.
[17] H.R. Reinhoudt, A.D. van Langeveld, R.M. Stockmann, R. Prins, H.W. Zandbergen, J.A. Moulijn, J. Catal. 179 (1998) 443.
[18] H.R. Reinhoudt, E. Crezee, A.D. van Langeveld, P.J. Kooyman, J.A.R. van Veen, J.A. Moulijn, J. Catal. 196 (2000) 315.
[19] H.R. Reinhoudt, R. Troost, A.D. van Langeveld, J.A.R. van Veen, S.T. Sie, J.A. Moulijn, J. Catal. 203 (2001) 509.
[20] M.J. Vissenberg, Y. van der Meer, E.J.M. Hensen, V.H.J. de Beer, A.M. van der Kraan, R.A. van Santen, J.A.R. van Veen, J. Catal. 198 (2001) 151.
[21] H.R. Reinhoudt, C.H.M. Boons, A.D. van Langeveld, J.A.R. van Veen, S.T. Sie, J.A. Moulijn, Appl. Catal. A 207 (2001) 25.
[22] J. Ramírez, A. Gutiérrez-Alejandre, Catal. Today 43 (1998) 123.
[23] A. Guevara-Lara, R. Bacaud, M. Vrinat, Appl. Catal. A 328 (2007) 99.
[24] A. Guevara, R. Bacaud, M. Vrinat, Appl. Catal. A 253 (2003) 515–526.
[25] R.J. Hunter, Zeta Potential in Colloid Science: Principles and Applications, Academic Press Inc., New York, 1981.
[26] A. Guevara, R. Bacaud, M. Vrinat, Actas XVII Simposio Ibero Americano de Catálisis 3 (2002) 1387.
[27] G. Deo, I.E. Wachs, J. Phys. Chem. 95 (1991) 5889.
[28] J.M. Stencel, Raman Spectroscopy for Catalysis, Van Nostrand Reinhold, New York, 1990.
[29] S. Cheng, M. Leuges, S. Bare, J. Phys. Chem. 96 (1992) 25.
[30] G.D. Panagiotou, T. Petsi, K. Bourikas, C. Kordulis, A. Lycourghiotis, J. Catal. 262 (2009) 266.
[31] A. Vurman, I.E. Wachs, A.M. Hirt, J. Phys. Chem. 95 (1991) 9928.
[32] S.S. Chan, I.E. Wachs, L.L. Murrell, N.C. Dispenziere Jr., J. Catal. 92 (1985) 1.
[33] J. Ramirez, L. Ruiz, L. Cedeno, V. Harle, M. Vrinat, M. Breysse, Appl. Catal. 93 (1993) 163.
[34] C. Lepetit, M. Che, J. Phys. Chem. 100 (1996) 3137.
[35] A.B. Lever, Inorganic Electronic Spectroscopy, Studies in Physical Theoretical Chemistry, 33, Elsevier, Amsterdam, 1984, 507.
[36] J.C. Carter, P.K. Khulbe, J. Gray, J.W. Van Zee, S.M. Angel, Anal. Chim. Acta 524 (2004) 241.
[37] H. Jeziorowski, H. Knözinger, J. Phys. Chem. 83 (1979) 1166.
[38] F. Iova, A. Trutia, Opt. Mater. 13 (2000) 455.
[39] M.L. Jocono, M. Schavello, A. Cimino, J. Phys. Chem. 75 (1971) 1044.
[40] S. Damyanova, A. Spojakina, K. Jiratova, Appl. Catal. A 125 (1995) 257.
[41] V.L.S.T. da Silva, F.P. Lima, L.C. Dieguez, M. Schmal, Ind. Eng. Chem. Res. 37 (1998) 82.
[42] V.L.S.T. da Silva, R. Frety, M. Schmal, Ind. Eng. Chem. Res. 33 (1994) 169.
[43] K.T. Ng, D.M. Hercules, J. Phys. Chem. 80 (1976) 2094.
[44] L. Coulier, G. Kishan, J.A.R. van Veen, J. Niemantsverdriet, J. Phys. Chem. B 106 (2002) 5897.
[45] L. Blanchard, J. Grimblot, J.P. Bonnelle, J. Catal. 98 (1986) 229.
[46] J.P. Espinos, A.R. Gonzalez-Elipe, G. Munuera, Solid State Ionics 63–65 (1993) 748.